Superhydrophobic Properties of Nanotextured Polypropylene Foils Fabricated by Roll-to-Roll Extrusion Coating

Telecka, Agnieszka; Murthy, Swathi; Sun, Ling; Pranov, Henrik; Taboryski, Rafael J.

Published in:
ACS Macro Letters

Link to article, DOI:
10.1021/acsmacrolett.6b00550

Publication date:
2016

Document Version
Peer reviewed version

Superhydrophobic properties of nanotextured polypropylene foils fabricated by roll–to–roll extrusion coating

Agnieszka Telecka[1], Swathi Murthy[2,3], Ling Schneider[1], Henrik Pranov[3], and Rafael Taboryski[*,1]

[1]Department of Micro- and Nanotechnology, Technical University of Denmark, 2800 Kongens Lyngby, Denmark

[2]Department of Photonics Engineering, Technical University of Denmark, Frederiksborgvej 399, DK-4000 Roskilde, Denmark

[3]Inmold A/S, Gregersensvej 6H, DK-2630 Taastrup, Denmark

* rata@nanotech.dtu.dk

Abstract

We demonstrate the use of roll-to-roll extrusion coating (R2R-EC) for fabrication of nanopatterned polypropylene (PP) foils with strong anti-wetting properties. The anti-wetting nanopattern is originated from textured surfaces fabricated on silicon wafers by a single-step method of reactive ion etching with different processing gas flow rates. We provide a systematic study of the wetting properties for the fabricated surfaces and show that a controlled texture stretching effect in the R2R-EC process is instrumental to yield the superhydrophobic surfaces with water contact angles approaching 160° and droplet roll-off angles below 10°.

Technologies for fabrication of biomimetic surfaces with superhydrophobic properties have gained considerable attention,[1, 2] due to the broad range of applications such as solar cells,[3] self–cleaning fabrics,[4] anti-reflective, anti-fogging,[5, 6] and anti–ice materials.[7] In nature, the superhydrophobic effect aka the lotus effect is mostly known from plant leafs[8], but is also encountered in fauna, e.g. the water strider Notonecta glauca[9, 10]. Fabrication of superhydrophobic materials usually require initial structuring with a hierarchical micro and nanopattern to increase surface roughness,[11, 12] and a subsequent coating with low surface energy chemistry[13, 14]. The surface coating does however represent at least one extra fabrication step and is best suited for coating of solid surfaces, such as that of Si with perfluorodecyltrichlorosilane (FDTS).[15] Enabling direct large-area surface texturing of intrinsically hydrophobic thermoplastics would be more feasible and lower the barrier for use of superhydrophobic materials for e.g. self-cleaning applications.

Among technologies for large-area nanotexturing, roll-to-roll (R2R) UV-assisted nanoimprint lithography is the most established. It was originally demonstrated by Ahn et al,[16, 17] and more recently by Leitgeb et al. with even faster roller speed in excess of 10 m/min on a 25 cm wide web.[18] This R2R method is feasible for nanostructuring but is limited with regard to surface chemistry, as the relief must be formed in a UV-curable resin. John et al. demonstrated R2R nanoimprinting using perfluoropolyether (PFPE) composite molds[19], while Li et al. reported production of large area flexible biomimetic surfaces using a R2R UV-assisted nanoimprint process[20]. The method employed by Li et al. requires steps of photocuring of the structured layer and coating. Moreover it runs at modest line-speed of 10 in/min (~0.25 m/min) with web width of 6 in (~150 mm). A R2R method for production of large area superhydrophobic surfaces should preferably have much higher productivity and allow structuring of common inexpensive and intrinsically hydrophobic polymers such as polyethylene,[21] cyclic olefin copolymer,[22] or polypropylene (PP)[23] to gain practical relevance. An ideal material is isotactic PP, which has good hydrophobic properties (see Table S1), has low surface energy and is inexpensive.[24]

In this paper we report on R2R extrusion coating (R2R-EC), as sketched in **Figure 1a**, for the manufacture of superhydrophobic surfaces in PP. In R2R-EC, the polymer melt curtain is extruded through a flat nozzle, then laminated onto a carrier foil by squeezing the melt between a cooling roller and a counter roller, and finally collected on a wind–up roller. In a previous publication, we demonstrated this method for replication of nanopillar structures in PP.[25] R2R-EC is well established and widely used in the packaging industry for large scale fabrication of smooth polymer films. However, to the best of our knowledge, nanotexturing of surfaces with biomimetic functionalities produced with R2R-EC has not yet been reported.

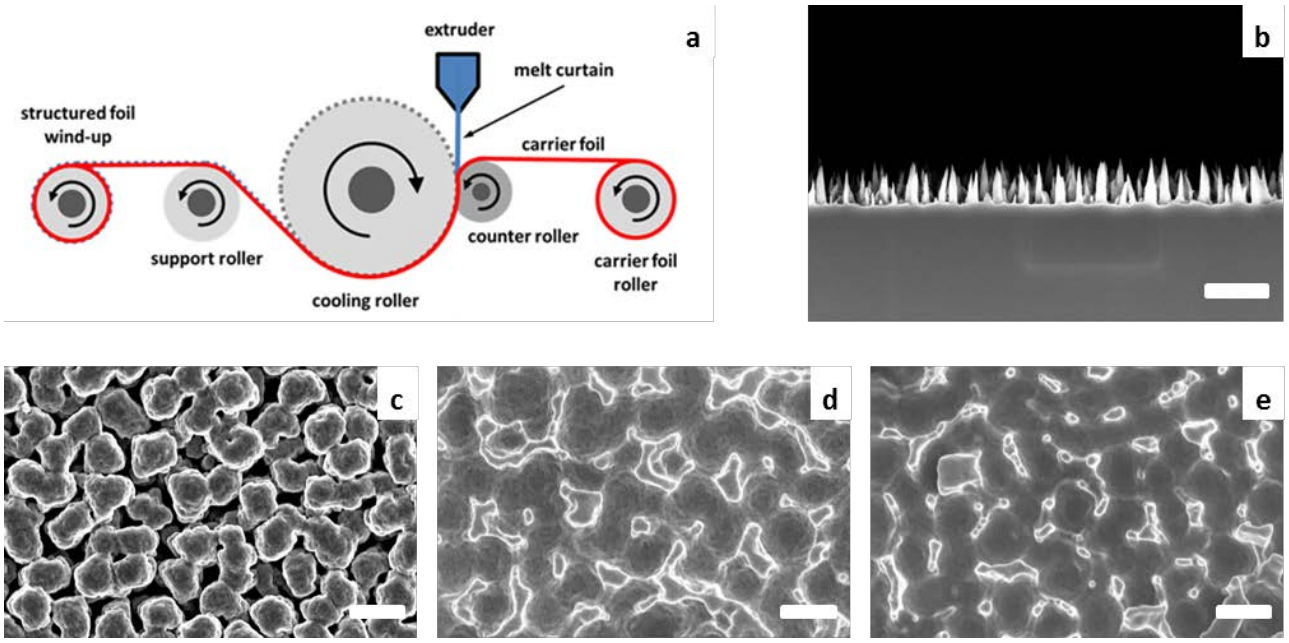

Fig.1 (a) Schematic representation of R2R EC process. **(b)** SEM image of the nanograss master features fabricated on Si wafer with the 70-70 process, cross section. **(c)** SEM image of the corresponding mold (70-70), top view. **(d)** SEM image, top view of PP foil with 70-70 replicated pattern, $T_C = 70°$, $V_R = 20$ m/min. **(e)** SEM image, top view of PP foil with 70-70 replicated pattern, $T_C = 70°$, $V_R = 60$ m/min. Scale bars for figures (b), (c), (d), and (e) are all 1 µm.

For the master structure, we use a Si nanograss texture.[26] The nanograss was originated in Si by reactive ion etching (RIE). RIE can be used for maskless texturing of silicon surfaces through the combined effect of a corrosive gas (SF_6 and/or CH_4) and a passivating gas (O_2).[27-31] Surfaces made this way predominantly appear black due to the scattering of the incident light by the surface texture. Hence, the texture is also known as "black silicon", and has widely been used for optical anti-reflective surfaces.[27, 30, 31] By tuning the processing parameters, it is possible to alter the structure shape.[32] The processing parameters used are shown in the Supplementary Information, Table S2. In this study all parameters were kept constant except for the oxygen gas flow rate, which was varied in order to optimize functionality. For simplicity, we denote samples of different SF_6 and O_2 flow rates as $Q_{SF_6} - Q_{O_2}$. Therefore 70-70 means a sample processed with Q_{SF_6}= 70 sccm, and Q_{O_2}= 70 sccm. The Si master structure was transferred to a Ni mold by electroforming a negative relief texture on top of the textured Si wafers. After removal of the Si by etching in potassium hydroxide, the Ni counterparts were attached to the cooling roller and used as molds for the replication step. The whole process sequence is sketched in **Figure S1** while SEM pictures of the Ni molds are shown in **Figure S2**. **Figure 1b** shows a scanning electron microscopy (SEM) image of the 70-70 Si master profile structure, while **Figure 1c** a set of top view SEM images of the mold for a 70-70 structure, and the corresponding replicated PP surfaces at line-speeds 60 m/min and 20 m/min. Details of the whole fabrication process are given in the Supplementary Information. Foils were produced at line speed ranging from 20 m/min to 60 m/min, while the cooling roller temperature T_C was kept at either 50° C or 70° C. The extruder screw speed was kept constant to produce a constant extruder output. This had the implication that the PP film thickness varied linearly with the line-speed from about 15 µm at 60 m/min to about 45 µm at 20 m/min. Hence, even the thinnest PP film is much thicker than the obtained structure heights. In **Figure 1c** we show the top view SEM images of respectively the mold surface, and the textured PP surfaces fabricated at line-speeds 60 m/min and 20 m/min.

We investigated the surface morphology of the fabricated foils by AFM imaging and observed that all surfaces fabricated with higher T_C (70° C) resulted in superior replication of features. Structures fabricated with $T_C = 50°$ C reached structure heights of only about 10 % of those fabricated at 70° C. Higher mold temperature makes the semi-crystalline PP less viscous, allowing it to flow more easily into the mold relief. This results in higher nanograss on the replicated foil surface. We will thus only discuss the performance of structures fabricated with $T_C = 70°$ C. For those surfaces, we found that the roughness parameter R_Z correlate with the roller line–speed V_R. R_Z is a standard roughness parameter defined in ISO 4278-1:1997 as the arithmetic mean value of the single roughness depths (the vertical distance between the highest peak and the deepest valley within the sampling length) of consecutive sampling lengths. We found that R_Z could be fitted to a sigmoidal function of V_R. The experimentally obtained $R_Z(V_R)$ dependence is shown in **Figure 2a** for the 70-70 structures together with the fitted sigmoidal function. Figure **2b** illustrates the stretching effect to be discussed below. **Figure 2c** shows 3d AFM images of the mold and the PP surfaces for the two extreme values of line-speed, while examples of the traces used to determine the R_Z values are shown in **Figure 2d**. We see that R_Z = (426 ± 36.6) nm for nanostructures replicated with V_R = 20 m/min, while R_Z = (240 ± 16.4) nm for V_R = 60 m/min. In order to assess the replication, we measured the R_Z value for the Ni mold by employing exactly the same procedure as for the PP samples and arrived at the value R_Z = (218 ± 9.4) nm. We notice that this R_Z value for the mold best corresponds to the smallest of values in **Figure 2a** obtained for high V_R, while for lower V_R we see R_Z values exceeding those of the mold by almost 100 %. Although the Ni mold has an inverted relief, R_Z is expected to match for mold and replica for a true replication. Thus the structure undergoes a tensile plastic deformation at low roller speed. Such stretching of structures has previously been reported for related fabrication technologies.[33-35] Further, when comparing with the Si master structure (**Figure 1b**), we see a reduction in texture height between Si master and Ni mold, which is caused by an unavoidable inhomogeneous current distribution at the dense surface of the random nanograss texture during the Ni electroforming process.

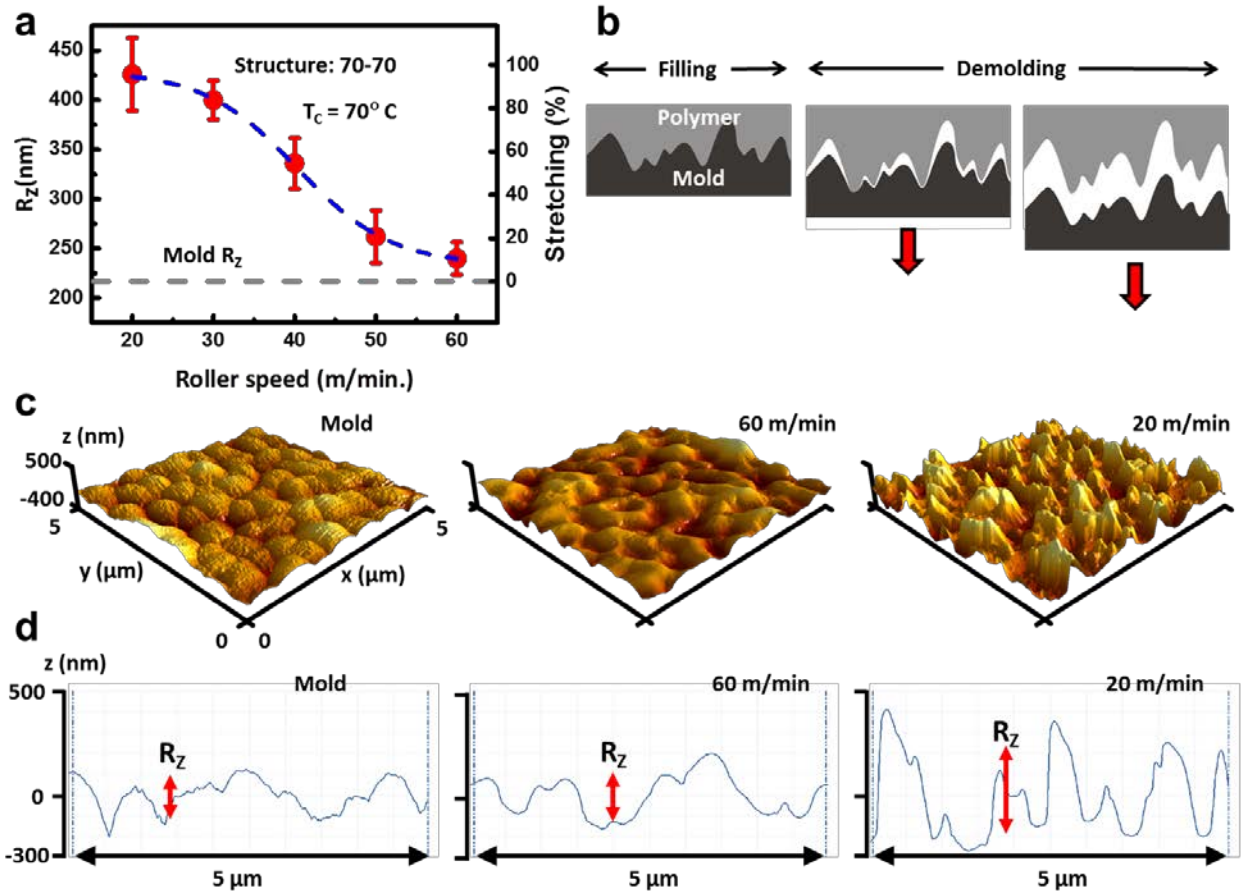

Fig.2 (a) Dependence of the R_Z parameter on roller line speed V_R for the 70-70 structure obtained at 70° C. The values were obtained as the mean values from four (two vertical and two horizontal) traces in the 5 µm x 5 µm evaluation area. Error bars are SD (n=4) between the four individual R_Z values acquired for each trace. The dotted horizontal line represents the R_Z value for the mold, and the right y-axis shows the percentage of stretching of the structures compared to the mold value. The fitted function is a sigmoidal Boltzmann function. **(b)** Schematic of the stretching during the demolding phase of the fabrication. **(c)** 3D AFM "true surface" data showing a comparison of the mold corresponding to the 70-70 structure, and the corresponding replicated PP surfaces fabricated with the two extreme values of roller speed 20 m/min and 60 m/min respectively. No axis scaling is applied. **(d)** Representative 2D AFM scan profiles for the mold and for polymer surfaces fabricated with20 m/min, and 60 m/min. The R_Z value is indicated in red for each

trace, and is obtained as the average of three peak-to-valley distances each from one of three subdivisions of the traces. Y-axis is the same for all traces.

In R2R-EC, a force is exerted on the compliant counter roller to form the so-called nip region where the molten polymer solidifies and adheres to the carrier foil. For a force F, applied to the counter roller, the nip pressure is given by:[36, 37]

$$P_{nip} = P_{max}\sqrt{1-\left(\frac{L_{nip}-2x}{L_{nip}}\right)^2}, \qquad (\mathbf{1})$$

where $P_{max} = F/(\pi W L_{nip})$, x is the distance along the roller inside the nip from the entrance of polymer melt, L_{nip} is the length of the nip region, and W is the width of the rollers. The nip length L_{nip} can be measured for the applied force F/W = 30 kN/m, and was L_{nip} = 18 mm. Hence, according to **Equation 1**, the max pressure in the nip is about 24 bar. For a higher line-speed, the polymer will reach further into the nip (larger x) and experience a higher pressure while being cooled to a given temperature. The residence time for the polymer inside the nip is thus simply given by L_{nip}/V_R. Hence, for V_R = 60 m/min, the polymer will spend 18 ms inside the nip, while for a lower line-speed (20 m/min), the polymer will pass through the pressure profile given by **Equation 1** over longer time (54 ms), and simultaneously cool more due to heat conduction. The thicker PP film obtained for higher roller speed is not enough to compensate for the extremely high cooling rate. The semi-crystalline nature of PP plays an important role in this rheological process, as considerable crystallization retardation is expected for the extremely high cooling rate (~10^7 K/s) near the mold.[25] This leads to texture replication while the polymer is in a supercooled state, and hence does not solidify despite the temperature rapidly drops below the normal solidification temperature.[38] Regarding the texture stretching effect at low V_R, the data indicate that almost no stretching occurs, when the polymer is less solidified during the demolding phase of the process, whereas

the tensile plastic deformation requires a higher degree of solidification that causes the polymer to stick to the mold.

The superhydrophobic effect relies on the so-called Cassie–Baxter[39] (CB) state, where the surface structures entrap air and thereby form a chemically heterogeneous interface consisting of air and solid to the water. On the macroscopic level, such surfaces are characterized by having WCA above 150° and small contact angle hysteresis (CAH).[40] In the CB state, sessile droplets will roll off a superhydrophobic surface for only a small tilt angle α.[26] Low roll–off angles thus provide a practical measure of the self–cleaning properties of the material.[15, 41] In the Cassie-Baxter model, the apparent WCA (θ_e) can be expressed by

$$\cos\theta_e = f_s(\cos\theta_Y + 1) - 1, \qquad (\mathbf{2})$$

where θ_Y is the Young contact angle, i.e. the contact angle for a smooth surface having the same surface chemistry, whereas $f_s = \frac{A_{ls}}{A_{ls}+A_{lg}}$ is the area fraction of the liquid solid interface area to that of the total area of both the liquid solid interface and the liquid gas interface. For the PP used in this study, we have θ_Y= (100.1 ± 2.2)°.

To analyze the impact of R_Z values on surface functionality we characterized wetting properties of nanopatterned PP foils fabricated with T_C = 70°. We conducted systematic contact angle measurements in static and dynamic mode to obtain advancing, receding and static water contact angles (WCA) and roll–off angles (α) for each surface. Since α depends on the droplet volume[42] all measurements were done using the same droplet volume of 10 µl. Among the analyzed nanograss textures, texture 70-70 exhibits the highest contact angles and lowest roll-off angles. For this nanostructure, recorded WCA exceed 150°. Foils replicated with pattern 70-90 achieved WCA in the range between 140° to 150°. For surfaces fabricated with the 70-50 morphology we observed the most uneven results. Here WCA ranged between 120° and 145° with huge variations. **Figure 3a** presents an overview of advancing WCA recorded for specific

replicated texture topographies in the whole range of line-speeds V_R, while all receding WCA results collected for replicated foils are presented in **Figure 3b**. In **Figure 3c**, we summarize the wetting properties for foils with 70-70 replicated texture by plotting the static contact angle data and the roll-off angle data for the 70-70 foils as a function of R_Z. The recorded values of α descend well below 20° while the WCA approaches 150° for the largest values of R_Z. Surfaces with 70-90 nanostructures resulted in higher α, ranging from 22° to 45° but for all droplets we eventually observed roll-off when tilting the surface. Only for foils fabricated with the 70-50 nanotexture we observed pinning of water drops, in some cases even for a tilt over 90°.

For structures 70-50, we tested the hypothesis of full wetting, i.e. that sessile droplets rest in the socalled Wenzel state. For this state, the apparent WCA θ_e is given by the Wenzel equation: $\cos\theta_e = r\cos\theta_Y$, where $r > 1$ is the ratio of the real surface area to the projected surface area, and θ_Y is the Young CA for the unstructured foil surface given above. r can readily be obtained from the AFM data (**Figure S8** and **Table S3)**. We see that the Wenzel equation fails to predict the measured WCA data, and we must conclude that even for the 70-50 surfaces, the droplets are in the Cassie-Baxter state.

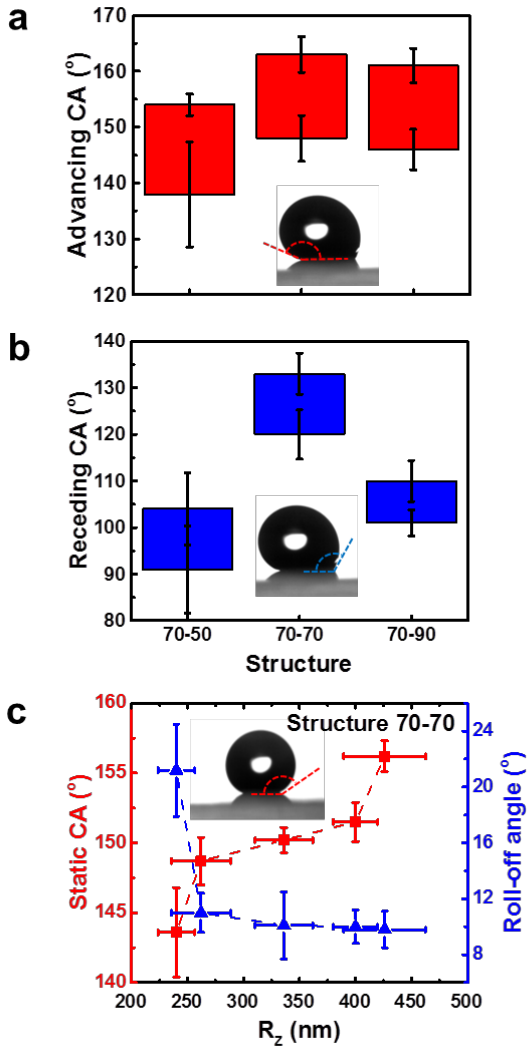

Fig.3 (a) Graph of advancing water CA recorded for specific replicated foils topographies in whole range of line speed V_R with the high values corresponding to low line-speed, and low the low values corresponding to high line-speeds. **(b)** Graph of receding WCA recorded for specific replicated foils topographies in whole range of line speed V_R. Error bars represent one SD (n=3) for both figures (a) and (b)**. (c)** Dependence of WCA and roll-off angle α on R_Z for foils fabricated with 70-70 nanostructure. The droplet volume used for all measurements was 10 µl.

On the microscopic level, the wetting of such surfaces can be characterized according to the degree of water intrusion into the structures.[26, 43, 44] The data in **Figure 3c** indicate a transition to an enhanced de-

wetting state roughly at R_Z = 325 nm. In a previous publication we found that the wetting properties for superhydrophobic surfaces with cone shaped structure depends on the opening angles of cones, rather than their heights.[26] However, when cones get stretched, their opening angle decreases. This is shown in **Figure 4**, where we plot the average opening angle of the structure as a function of the R_Z values obtained as a result of different roller line-speeds. The opening angles were derived from the Root Mean Square Gradient, Sdq obtained from the AFM data, $Sdq = \sqrt{\frac{1}{A}\iint((\partial z/\partial x)^2 + (\partial z/\partial y)^2)dxdy}$, where A is the sampling area. The average opening angle $\tilde{\alpha}_{oa}$ is then obtained as $\tilde{\alpha}_{oa} = 2\cot^{-1}(Sdq)$. $\tilde{\alpha}_{oa}$ is not exactly the same as the opening angle of spikes in contact with the water interface, however, the two very likely have the same dependence on R_Z. We can thus argue that our data are consistent with the wetting properties being determined by either the height or the opening angles of the nanograss cones. A more fundamental argument can be given that most probably it is the opening angle that is the dominating parameter for wetting, since sessile droplets on a superhydrophobic surface will wet only the summits of the structure irrespective of their height.

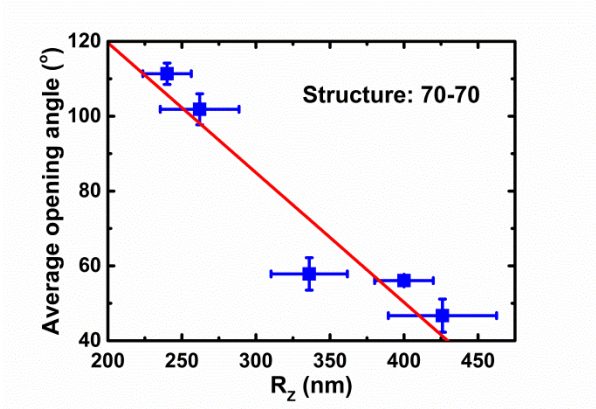

Fig.4 Plot of the average opening angle of cones vs. R_Z for foils fabricated with 70-70 at $T_C = 70°$ C. The dashed red trend line is added to guide the eye. Error bars represent one standard deviation (n=4).

In conclusion, we have demonstrated the superhydrophobic effect for nanostructured polymer surfaces fabricated with a high throughput and low cost novel R2R-EC method.. We obtained the most pronounced

anti-wetting effect for the highest textures obtained by exploiting a controlled tensile plastic deformation of the nano-texture through systematic adjustment of the cooling roller temperature T_C and roller line-speed V_R. The most stretched structures turned out to have the smallest opening angles and were obtained for the lowest roller speed. This let us to the conclusion that the strongest superhydrophobic effect with WCA approaching 160°, and with roll-off angles below 10°, was obtained for structures having the lowest opening angle resulting from the stretching effect.

Author Contributions

RT conceived the project. AT, LS, SM, and HP performed the experiments. AT made the data analysis. AT and RT wrote the manuscript with comments from all authors. Approval of the final version was given by all authors.

Acknowledgements

This work was supported by The Danish Ministry of Higher Education and Science, through an industrial PhD scholarship for SM (grant 1355-00143), and by the Technical University of Denmark, through a special PhD stipend for AT for collaboration with partner universities.

References

1. Xue, C.-H.; Jia, S.-T.; Zhang, J.; Ma, J.-Z., Large-area fabrication of superhydrophobic surfaces for practical applications: an overview. *Science and Technology of Advanced Materials* **2010,** *11* (3).
2. Yan, Y. Y.; Gao, N.; Barthlott, W., Mimicking natural superhydrophobic surfaces and grasping the wetting process: A review on recent progress in preparing superhydrophobic surfaces. *Advances in Colloid and Interface Science* **2011,** *169* (2), 80-105.
3. Leem, J. W.; Kim, S.; Lee, S. H.; Rogers, J. A.; Kim, E.; Yu, J. S., Efficiency Enhancement of Organic Solar Cells Using Hydrophobic Antireflective Inverted Moth-Eye Nanopatterned PDMS Films. *Advanced Energy Materials* **2014,** *4* (8).
4. Caschera, D.; Cortese, B.; Mezzi, A.; Brucale, M.; Ingo, G. M.; Gigli, G.; Padeletti, G., Ultra Hydrophobic/Superhydrophilic Modified Cotton Textiles through Functionalized Diamond-Like Carbon Coatings for Self-Cleaning Applications. *Langmuir* **2013,** *29* (8), 2775-2783.
5. Anastasiadis, S. H., Development of Functional Polymer Surfaces with Controlled Wettability. *Langmuir* **2013,** *29* (30), 9277-9290.
6. Li, J.; Zhu, J.; Gao, X., Bio-Inspired High-Performance Antireflection and Antifogging Polymer Films. *Small* **2014,** *10* (13), 2578-2582.
7. Kulinich, S. A.; Farzaneh, M., Ice adhesion on super-hydrophobic surfaces. *Applied Surface Science* **2009,** *255* (18), 8153-8157.

8. Barthlott, W.; Neinhuis, C., Purity of the sacred lotus, or escape from contamination in biological surfaces. *Planta* **1997,** *202* (1), 1-8.
9. Gao, X. F.; Jiang, L., Water-repellent legs of water striders. *Nature* **2004,** *432* (7013), 36-36.
10. Ditsche-Kuru, P.; Schneider, E. S.; Melskotte, J.-E.; Brede, M.; Leder, A.; Barthlott, W., Superhydrophobic surfaces of the water bug Notonecta glauca: a model for friction reduction and air retention. *Beilstein Journal of Nanotechnology* **2011,** *2*, 137-144.
11. Nosonovsky, M.; Bhushan, B., Biologically inspired surfaces: Broadening the scope of roughness. *Advanced Functional Materials* **2008,** *18* (6), 843-855.
12. Bell, M. S.; Shahraz, A.; Fichthorn, K. A.; Borhan, A., Effects of Hierarchical Surface Roughness on Droplet Contact Angle. *Langmuir* **2015,** *31* (24), 6752-6762.
13. Yeh, K.-Y.; Chen, L.-J.; Chang, J.-Y., Contact angle hysteresis on regular pillar-like hydrophobic surfaces. *Langmuir* **2008,** *24* (1), 245-251.
14. Zhang, L.; Zhou, Z.; Cheng, B.; DeSimone, J. M.; Samulski, E. T., Superhydrophobic behavior of a perfluoropolyether lotus-leaf-like topography. *Langmuir* **2006,** *22* (20), 8576-8580.
15. Larsen, S. T.; Andersen, N. K.; Sogaard, E.; Taboryski, R., Structure Irregularity Impedes Drop Roll-Off at Superhydrophobic Surfaces. *Langmuir* **2014,** *30* (17), 5041-5045.
16. Ahn, S. H.; Guo, L. J., High-speed roll-to-roll nanoimprint lithography on flexible plastic substrates. *Advanced Materials* **2008,** *20* (11), 2044-+.
17. Ahn, S. H.; Guo, L. J., Large-Area Roll-to-Roll and Roll-to-Plate Nanoimprint Lithography: A Step toward High-Throughput Application of Continuous Nanoimprinting. *Acs Nano* **2009,** *3* (8), 2304-2310.
18. Leitgeb, M.; Nees, D.; Ruttloff, S.; Palfinger, U.; Götz, J.; Liska, R.; Belegratis, M. R.; Stadlober, B., Multilength Scale Patterning of Functional Layers by Roll-to-Roll Ultraviolet-Light Assisted Nanoimprint Lithography. *ACS Nano* **2016,** *DOI: 10.1021/acsnano.5b07411*.
19. John, J.; Tang, Y.; Rothstein, J. P.; Watkins, J. J.; Carter, K. R., Large-area, continuous roll-to-roll nanoimprinting with PFPE composite molds. *Nanotechnology* **2013,** *24* (50).
20. Li, Y.; John, J.; Kolewe, K. W.; Schiffman, J. D.; Carter, K. R., Scaling Up Nature: Large Area Flexible Biomimetic Surfaces. *Acs Applied Materials & Interfaces* **2015,** *7* (42), 23439-23444.
21. Puukilainen, E.; Rasilainen, T.; Suvanto, M.; Pakkanen, T. A., Superhydrophobic polyolefin surfaces: Controlled micro- and nanostructures. *Langmuir* **2007,** *23* (13), 7263-7268.
22. Khan, A.; Li, S.; Tang, X.; Li, W.-D., Nanostructure transfer using cyclic olefin copolymer templates fabricated by thermal nanoimprint lithography. *Journal of Vacuum Science & Technology B* **2014,** *32* (6).
23. Huovinen, E.; Takkunen, L.; Suvanto, M.; Pakkanen, T. A., Fabrication and quantitative roughness analysis of hierarchical multiscale polymer surface structures. *Journal of Micromechanics and Microengineering* **2014,** *24* (5).
24. Erbil, H. Y.; Demirel, A. L.; Avci, Y.; Mert, O., Transformation of a simple plastic into a superhydrophobic surface. *Science* **2003,** *299* (5611), 1377-1380.
25. Murthy, S.; Matschuk, M.; Huang, Q.; Mandsberg, N. K.; Feidenhans'l, N. A.; Johansen, P.; Christensen, L.; Pranov, H.; Kofod, G.; Pedersen, H. C.; Hassager, O.; Taboryski, R., Fabrication of Nanostructures by Roll-to-Roll Extrusion Coating. *Advanced Engineering Materials* **2016,** *18* (4), 484-489.
26. Schneider, L.; Laustsen, M.; Mandsberg, N.; Taboryski, R., The Influence of Structure Heights and Opening Angles of Micro- and Nanocones on the Macroscopic Surface Wetting Properties. *Scientific Reports* **2016,** *6*.
27. Sainiemi, L.; Jokinen, V.; Shah, A.; Shpak, M.; Aura, S.; Suvanto, P.; Franssila, S., Non-Reflecting Silicon and Polymer Surfaces by Plasma Etching and Replication. *Advanced Materials* **2011,** *23* (1), 122-+.
28. Dagostino, R.; Flamm, D. L., PLASMA-ETCHING OF SI AND SIO2 IN SF6-O2 MIXTURES. *Journal of Applied Physics* **1981,** *52* (1), 162-167.

29. Jansen, H.; Deboer, M.; Burger, J.; Legtenberg, R.; Elwenspoek, M., THE BLACK SILICON METHOD .2. THE EFFECT OF MASK MATERIAL AND LOADING ON THE REACTIVE ION ETCHING OF DEEP SILICON TRENCHES. *Microelectronic Engineering* **1995,** *27* (1-4), 475-480.
30. Nguyen, K. N.; Basset, P.; Marty, F.; Leprince-Wang, Y.; Bourouina, T., On the optical and morphological properties of microstructured Black Silicon obtained by cryogenic-enhanced plasma reactive ion etching. *Journal of Applied Physics* **2013,** *113* (19).
31. Yue, Z.; Shen, H.; Jiang, Y., Antireflective nanostructures fabricated by reactive ion etching method on pyramid-structured silicon surface. *Applied Surface Science* **2013,** *271*, 402-406.
32. Dorrer, C.; Ruehe, J., Wetting of silicon nanograss: From superhydrophilic to superhydrophobic surfaces. *Advanced Materials* **2008,** *20* (1), 159-+.
33. Roehrig, M.; Mail, M.; Schneider, M.; Louvin, H.; Hopf, A.; Schimmel, T.; Worgull, M.; Hoelscher, H., Nanofur for Biomimetic Applications. *Advanced Materials Interfaces* **2014,** *1* (4).
34. Kavalenka, M. N.; Vuelliers, F.; Lischker, S.; Zeiger, C.; Hopf, A.; Roehrig, M.; Rapp, B. E.; Worgull, M.; Hoelscher, H., Bioinspired Air-Retaining Nanofur for Drag Reduction. *Acs Applied Materials & Interfaces* **2015,** *7* (20), 10651-10655.
35. Stormonth-Darling, J. M.; Pedersen, R. H.; How, C.; Gadegaard, N., Injection moulding of ultra high aspect ratio nanostructures using coated polymer tooling. *Journal of Micromechanics and Microengineering* **2014,** *24* (7).
36. Sollogoub, C.; Felder, E.; Dernay, Y.; Agassant, J. F.; Deparis, P.; Mikler, N., Thermomechanical analysis and modeling of the extrusion coating process. *Polymer Engineering and Science* **2008,** *48* (8), 1634-1648.
37. Hertz, H., Ueber die Berührung fester elastischer Körper. *J. Reine und Angewandte Mathematik* **1882,** *92*.
38. Gradys, A.; Sajkiewicz, P.; Minakov, A. A.; Adamovsky, S.; Schick, C.; Hashimoto, T.; Saijo, K., Crystallization of polypropylene at various cooling rates. *Materials Science and Engineering a-Structural Materials Properties Microstructure and Processing* **2005,** *413*, 442-446.
39. Cassie, A. B. D.; Baxter, S., Wettability of porous surfaces. *Transactions of the Faraday Society* **1944,** *40*, 0546-0550.
40. Chen, W.; Fadeev, A. Y.; Hsieh, M. C.; Oner, D.; Youngblood, J.; McCarthy, T. J., Ultrahydrophobic and ultralyophobic surfaces: Some comments and examples. *Langmuir* **1999,** *15* (10), 3395-3399.
41. Feng, X.; Jiang, L., Design and creation of superwetting/antiwetting surfaces. *Advanced Materials* **2006,** *18* (23), 3063-3078.
42. Furmidge, C. G., STUDIES AT PHASE INTERFACES .1. SLIDING OF LIQUID DROPS ON SOLID SURFACES AND A THEORY FOR SPRAY RETENTION. *Journal of Colloid Science* **1962,** *17* (4), 309-&.
43. Sogaard, E.; Andersen, N. K.; Smistrup, K.; Larsen, S. T.; Sun, L.; Taboryski, R., Study of Transitions between Wetting States on Microcavity Arrays by Optical Transmission Microscopy. *Langmuir* **2014,** *30* (43), 12960-12968.
44. Bottiglione, F.; Di Mundo, R.; Soria, L.; Carbone, G., Wenzel to Cassie Transition in Superhydrophobic Randomly Rough Surfaces. *Nanoscience and Nanotechnology Letters* **2015,** *7* (1), 74-78.

Key words

Roll-to-roll, extrusion coating, superhydrophobic, nanotexture, black silicon, polypropylene, crystallization retardation

Table of contents graphic

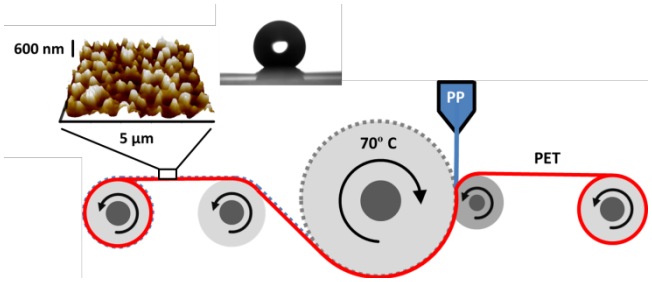

For Table of Contents Only